Original Article

STRUCTURAL, PHYSICAL, SURFACE AND NMR STUDY OF 5-(BENZYLTHIO)-1*H*-TETRAZOLE COMPOUND

Ravish Kumar Uppadhayay[1], Ashish Kumar[1], Jayant Teotia[1*], Isha Rathi[1], Pratima Singh[2], Syed Kashif Ali[3*]

[1]Molecular Spectroscopy and Biophysics Lab, Department of Physics, Deva Nagri College, Meerut-250002, India.
[2]Department of Chemistry, Digvijay Nath Post Graduate College, Gorakhpur-273001, India.
[3]Department of Chemistry, Faculty of Science Jazan University, Jazan-114, Saudi Arabia.
*Corresponding authors: jayant.phy@gmail.com, skali@jazanu.edu.sa

DOI: 10.47750/pnr.2022.13.S07.661

Abstract

Tetrazoles are involved in many pharmacological agents due to the carboxylic acid bioisoster. Despite their adjacent acidity, tetrazoles are further liphofilic than the agreeing carboxylate and are ionized at physiological potential for hydrogen (pH). Tetrazoles have gotten a lot of consideration because of their wide range of claims in coordination chemistry, medicinal chemistry and pharmaceutical sciences as well as materials science, including oxygen-containing fuels. They can be used as precursors for a variety of nitrogen-containing compounds, such as triazoles and thiazoles. Because of their wide range of applications, research into the catalytic preparation of tetrazoles has piqued the interest of many people. In particular, 1 -substituted tetrazole derivatives have been the subject of fundamental research due to their biological and medical applications. 5-(Benzylthio)-1*H*-tetrazole (5B1HT) was synthesized in this study. Powder XRD, FT-IR, FT-Raman, SEM, UV-Vis and NMR spectroscopy techniques were used to characterize it. The FT-IR, ^{1}H-NMR and ^{13}C-APT spectral measurements of the synthesized compound were discussed, as well as the complete assignment of the vibrational bands observed in spectra. Following full structure optimization and force field calculations based on density functional theory (DFT) at 6-311++G(d,p), cc-pVDZ basis sets, the spectra were interpreted using normal coordinate analysis. The total energy distribution, harmonic vibrational frequencies and IR intensities were determined using optimized geometry with both basis sets. The novelty of this paper is to study the properties of 5-(benzylthio)-1*H*-tetrazole (5B1HT) compound in its pure form.

Keywords: 5-(Benzylthio) -1*H*-tetrazole, PXRD, NMR, SEM, DFT study.

1. Introduction

Tetrazoles are a considerable heterocyclic compound with numerous industrial applications and scientific research in coordination chemistry [1], medicinal chemistry [2] and pharmaceutical sciences [3] as well as materials science, including oxygen-containing fuels [4-6]. Because of their practical applications, tetrazole and its derivatives have received a lot of (CN_4H_2) attention [7]. The tetrazolic acid fragment is almost isosteric with the carboxylic -CN_4 H acid group in terms of acidity [8]. However, it is biochemically more stable as COOH. As a result, one of the primary goals of -CN_4H research is to replace -CO_2H groups with groups from biologically active compounds [9]. Undeniably, the numeral of patent rights and journals related to tetrazole therapeutic uses is rapidly increasing and covers an extensive range of applications: Tetrazoles have been shown to have anti-hypertensive [10], anti-allergic and anti-biotic activity [11] and they are now used as anti-convulsant, as well as in cancer and AIDS dealing [12,13]. Tetrazoles are also used in agribusiness [14] as organic amendments [15],

pesticides [16] and insecticides [17], as stabilizing agents [18] in cinematography [19] and photo imaging [20] and as gas generators in airbags [21-24].

More notably, tetrazole is a particularly fascinating molecule because it has been demonstrated to exhibit the tautomerism depicted in Fig. 1. Tetrazole was discovered to occur solely as its '1H-tautomer' in the crystalline phases [25-27]. In solution, however, '1H- and 2H'-tautomers coexist, with the cohort of the most polar 1H-form operating at high solvent polarity [28,29]. The solvent effects on the tautomeric equilibrium were theoretically estimated using the 'self-consistent reaction field' (SCRF) model [30] and it was predicted that in media with dielectric constants less than approximately 7, 2*H*-tetrazole would be the least energy tautomer, even though in media with relatively large dielectric materials, an energy reversal occurs and 1*H*-tetrazole becomes the tautomeric ground state. The aim of this paper is to communicate the properties of 5-(benzylthio)-1*H*-tetrazole (5B1HT) compound in its pure form. The structure of 5B1HT along with the numbering of atoms are shown in Fig.1.2. There is currently no report based on its pure compound. Furthermore, DFT calculations are used to analyze the conformational, structural and vibrational properties of the 5B1HT molecule using the B3LYP functional with 6-311++G(d,p) and cc-pVDZ basis sets. The minimum energy conformational geometries were performed in the conformational analysis using a potential energy surface scan. The harmonic force field with the Pulay's scaled quantum mechanics force field (SQMFF) methodology was used to complete the report of the bands encountered in the vibrational spectra, taking into consideration the natural internal coordinates for the more stable structures.

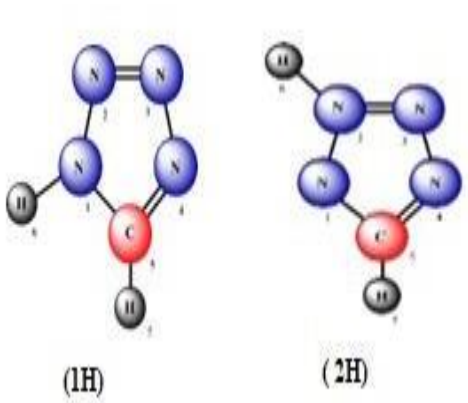

Fig.1. Tautomers of 5-substituted tetrazoles

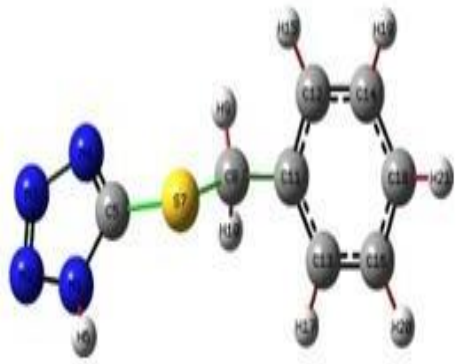

Fig. 1.2. Structure of 5-(Benzylthio)-1H-tetrazole molecule.

2. Synthesis of 5-(benzylthio)-1*H*-tetrazole [5B1HT]

We used a 250-mL doubled-necked flask equipped with a reflux condenser to prepare a suspension of triethylammonium chloride '$C_6H_{16}ClN$' (0.70 g, 0.005 mol) in toluene 'C_7H_8' (50 mL). The sodium azide 'NaN_3' (0.35 g, 0.005 mol) was then gradually added in portions while stirring. Toluene (50 mL) was gradually added and stirred for 15 min before being heated to gentle reflux for 18-20 h. After cooling the reaction mixture, 30 mL of distilled water was added to separate the aqueous layer. The toluene layer was then washed thoroughly and white crude extract was accumulated. After cooling to room temperature, the aqueous layer was acidified for 15 min with dilute HCl to pH 3-4 while stirring the mixture. The formed solid precipitate was collected, washed with water, crystallized from ethanol and vacuum-dried [31]. Yield 85.67 %, m.p.: 138.0-139.9 °C, IR (KBr $_{max}$, cm^{-1}): 3548 (–N–H), 3027.7 (aromatic –C=C–H), 2988 (aliphatic –C–H), 1536, 1453 (–C=C), 1394 (–N=N), 1546 (aromatic –C=C), ^{1}H NMR (300 MHz, $CDCl_3$) δ: 13.40-11.50 (s, 1H –N–H), 7.49-7.35 (m, 5H Ar–H), 4.58 (s, 1H –S–CH_2).

2.1. Experiment specifics

All of the chemicals and solvents used were reagent grade (Aldrich or Sigma) and had not been purified. further. PW1830 Philips analytical X-ray diffractometer (PXRD) with nickel filtered CuK (=0.154 nm) radiation was used to examine the synthesized 5B1HT (35 kV, 30 mA). The specimens were scanned at a scan rate of 0.02°/s for an angular range of 10°-70° of 2. Vibrational studies (3500- 100 cm^{-1}) were carried out using an FT-Raman spectrometer (Perkin Elmer GX 2000) with a resolution of 5 cm^{-1}. UV-Vis spectra were recorded in the wavelength range from 200 to 500 nm using a Jasco, V-570 UV-VIS Spectrophotometer. IR spectrum (3500-500 cm^{-1}) was recorded using KBr disc on a Mattson 1000 FT-IR spectrometer and reported in cm^{-1} units. ^{1}H and ^{13}C-NMR spectra were recorded on a Bruker spectrometer (300 MHz for 1H-NMR and 75 MHz for 13C-NMR). SEM Microscopy studies were carried out on JEOL, JSM-67001.

2.2. Computational details

Gaussian 09 software was used to perform the Density Functional Theory calculations, which included gradient geometry optimization [32,33]. The potential energy surface of the 5B1HT molecule was scanned with MMFF simulations to find the stable conformers. Conformational analysis was performed using the Spartan 10 program [34], and all conformational geometry was optimized using the Gaussian 09 program package with B3LYP/6-311++G(d,p) and B3LYP/cc–pVDZ basis sets. The most stable geometry of the 5B1HT molecule has been determined. Nuclear Magnetic resonance, Vibrational frequency calculations at the DFT level were performed using the optimized geometry of the most stable conformer. The DFT method B3LYP with 6-311++G(d,p) and cc-pVDZ basis sets were used in this study to compute all molecular properties of optimized structures. The vibrational modes for B3LYP/6-311++G(d,p) were assigned using the SQM program based on TED analysis [35].

The NMR analysis was carried out using the Gauge Independent Atomic Orbital (GIAO) method. Theoretical chemical shifts are compared to experimental results in order to identify and characterize the 5B1HT molecule. The chemical shifts of the most stable conformer of the 5B1HT molecule were calculated using the B3LYP functional with the 6-311++G(d,p) basis set. The calculations were carried out in DMSO solution with the IEF-PCM model. Theoretical and experimental chemical shifts in DMSO solution agree [36-40].

3. Experimental results and discussion:

3.1. Structural and optical study of [5-(benzylthio)-1*H*-Tetrazole] 5B1HT compound

5-(benzylthio)-1*H*-Tetrazole is found to be crystalline in nature [41] shown in Powder X-RD graph in Fig. 2. The graph has strong peak in the 2θ value of 17.14° with high intensity around at 18,028. Crystallinity of the material [42] is calculated by the using equation:

$$crystallinity\ Index = \frac{Area\ of\ crystalline\ peaks}{Area\ of\ all\ crystalline\ and\ amorphous\ peaks} \qquad \text{Eq(1)}$$

The calculated crystallinity obtained is ~51.15. High crystalline peaks in the same phase reveals the purity of the synthesized sample [43].

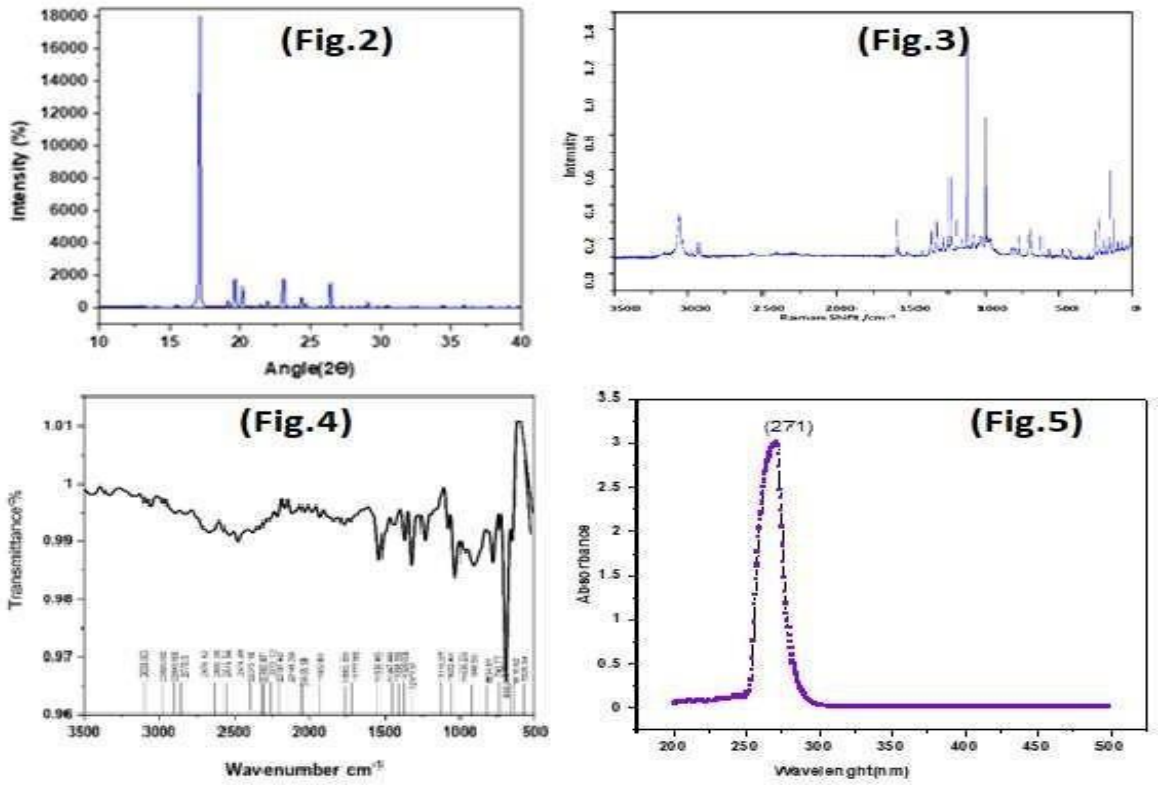

Fig. 2. Powder X-RD, Fig. 3 FT-RAMAN, Fig. 4. FT-IR (Vibrational study) Fig. 5. UV-Vis Spectroscopy analysis of 5B1HT compound.

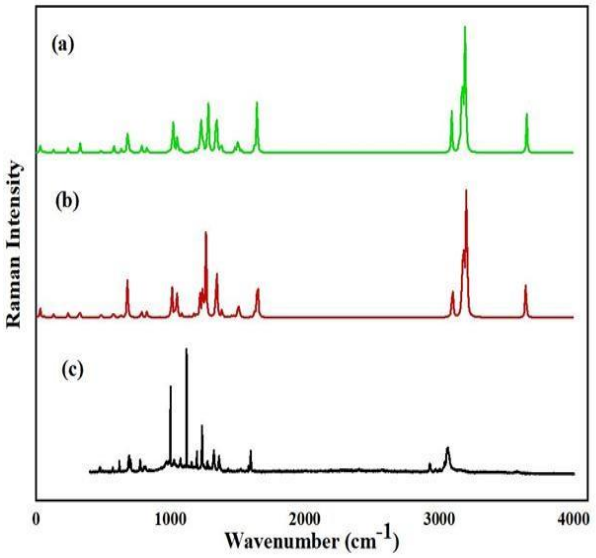

Fig. 3.1 FT-Raman spectra of 5B1HT (a) B3LYP/6-311++G(d,p) (b) B3LYP/aug-cc-pVDZ and (c) Experimental

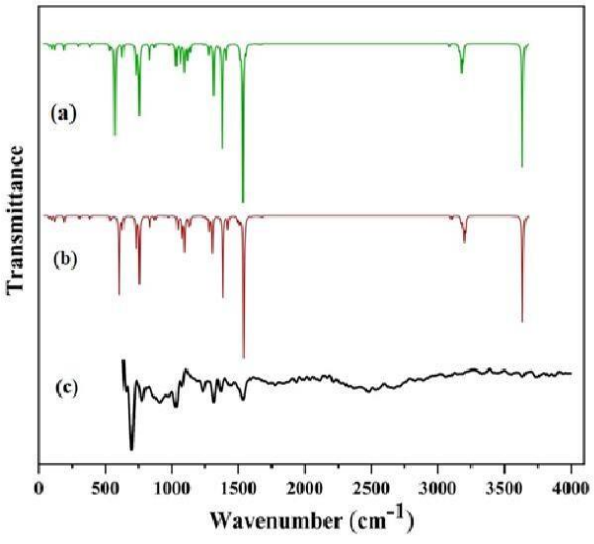

Fig. 4.1. FT-IR spectra of 5B1HT (a) B3LYP/6-311++G(d,p) (b) B3LYP/aug-cc-pVDZ and (c) Experimental

Fig. 3 shows the experimental FT-Raman spectrum of 5B1HT. Fig 3.1 shows FT-Raman spectra of 5B1HT at (a) B3LYP/6-311++G(d,p) (b) B3LYP/aug-cc-pVDZ and (c) Experimental. Fig. 4 shows the experimental FT-IR spectrum of 5B1HT. Fig 4.1 shows FT-IR spectra of 5B1HT at (a) B3LYP/6-311++G(d,p) (b) B3LYP/aug-cc-pVDZ and (c) Experimental. Sokolova et al. reported the crystalline phase (α-crystal) at room temperature for the first time in 1975 [44]. The precise behaviour of the crystalline phase under investigation could be easily confirmed by analysing the Raman spectrum's lower frequency spectral region (Fig.3.). Below 500 cm^{-1}, the recognized bands are 107.9 cm^{-1} with a head in the 110-121 cm^{-1} region, 136 and 169 cm^{-1} with a shoulder at

180 cm^{-1}, and the peaks shown are undistinguishable with those formerly testified by and Baglin in 1972 [45], illustrating that the identified pattern is coherent with the 'P1 space group,' which is the defining attribute of the -phase triclinic crystalline diverse array [46-48]. Bugalho et al. (2001) [49] confirmed the findings. In the Raman spectrum, l(N-H) is expected to be much less intense and is attributed to a set of weak broad bands with main intensities consolidated in the 3200-2900 cm^{-1} region. The assignment of the N-H out-of-plane bending, on the other hand, was not as simple. Because it is directly affected by inter-molecular connections, we can assume this mode to produce comparatively broader bands [50].

Fig. 5, absorption spectroscopy is a powerful tool for investigating the optical properties of a newly synthesized compound. Once it relates to un-substituted tetrazoles, UV-Vis spectroscopy is of little use because they absorb the most in the vacuum UV region (π- π^* < 200 nm) [51]. When dissolved in DMSO, a single absorbance peak at 271 nm is obtained, as shown in Fig. 5. This shift is caused by the bathochromic effect, which is influenced by intermolecular interactions and shifts the signals to a more useful UV region [52,53].

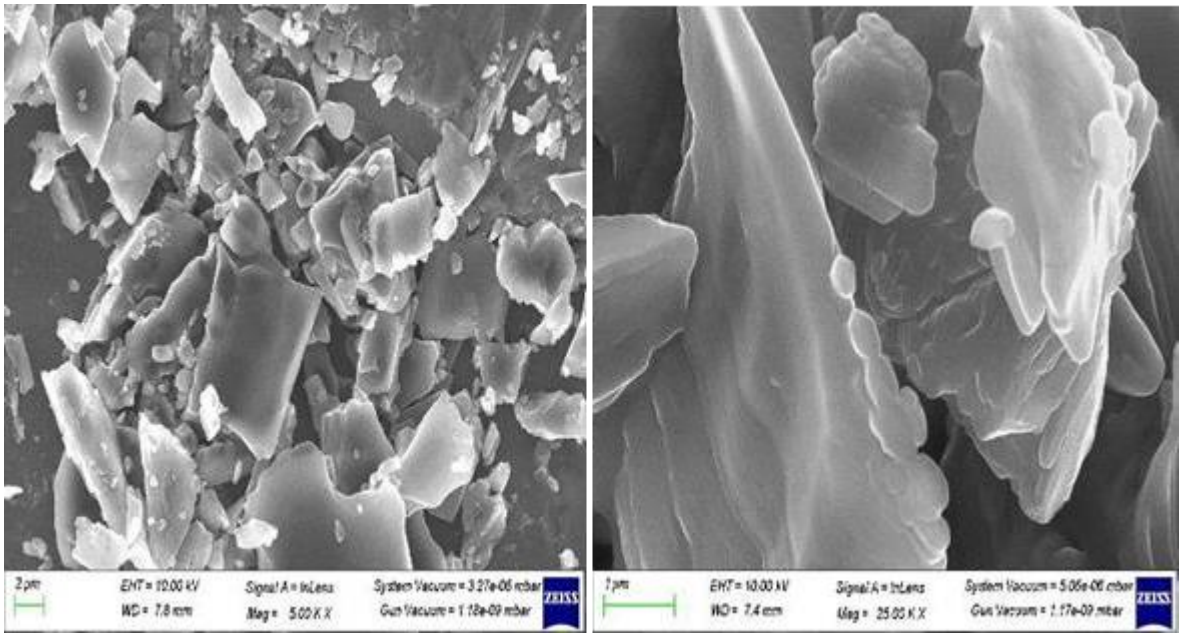

Fig. 6. SEM microscopic images of synthesized 5B1HT.

Fig. 6, microscopy images of the synthesized compound are shown. The lack of agglomeration in these images can be attributed to the strong carbon, hydrogen and nitrogen bonding that exists between them [54].

3.2. Vibrational study

The molecule 5-(Benzylthio)-1H-tetrazole (5B1HT) has 21 atoms which result in 3×21−6 = 57 modes of vibration. The vibrational spectral study of the molecule is analyzed by FT-IR and FT-Raman both experimentally and theoretically by DFT calculations using B3LYP/aug-cc-pVDZ and B3LYP/6-311++G(d,p) basis sets. The wavenumbers of various vibrational modes are obtained from the FT-IR and FT-Raman spectra. It is observed that the wavenumbers obtained by DFT calculations are overestimated as compared to experimental values. To match the theoretical wavenumbers with the experimental ones, appropriate scaling factors are used for both the basis sets. The scaling factor f is given by $f = \sum (ve \times vt) / \sum (vt2)$, where ve is the experimental wavenumber and vt is the theoretical wavenumber. The scaling factor for B3LYP/aug-cc-pVDZ basis set is 0.970 and for the B3LYP/6-311++G(d,p) basis set is 0.967. The vibrational experimental frequency (wavenumber), scaled and unscaled theoretical wavenumbers on both the basis sets along with detailed vibrational assignments are given in Table 1. The vibrational assignments show the percentage of stretching, in–plane bending, out–of–plane bending and torsion at each observed vibrational wavenumber. These assignments are based on potential energy distribution in which contributions greater than 10% are shown in the last column of Table 1. Out of the 57 modes of vibrations, 20 modes are of stretching, 19 modes are of bending and 18 modes are of torsion but most of the modes are a mixture of various types of vibrations.

In the aromatic ring, the C–C stretching (ν) vibrations are observed in the region 1700–1500 cm^{-1}. In Table 1, the C–C stretching are observed at mode number 9, 10, 18, 21, 28 and 30. In 5B1HT, the C–C stretching vibrations are observed at 1710, 1603 and 11016 cm^{-1} in the FTIR spectrum and at 1613 cm^{-1} in the FT–Raman spectrum. The scaled C–C stretching vibrations are also observed theoretically at 1590, 1570, 1295, 1185, 1014 and 984 cm^{-1} in 6-311++G(d,p) basis set and at 1598, 1577, 1300, 1183, 1016 and 980 cm^{-1} in aug-cc-pVDZ basis set. The in–plane bending mode for C–C–C vibrations is observed at mode number 28, 30 and 37. All the three modes are observed along with C–C stretching vibrations. The C–C stretching vibrations are observed at 1016 cm^{-1} in the FTIR spectrum and at 984 and 799 cm^{-1} in 6-311++G(d,p) basis set and at 980 and 800 cm^{-1} in aug-cc-pVDZ basis set. The C–C–C torsion vibrational mode are observed at mode number 31, 33, 34, 36, 38 and 40. The C–C–C torsion is observed at 976, 951, 925 and 759 cm^{-1} in the IR spectrum and at 893 and 727 cm^{-1} in the Raman spectrum. The scaled C–C–C torsion vibrations are also observed theoretically at 970, 953, 903, 827, 759 and 686 cm^{-1} in 6-311++G(d,p) basis set and at 969, 951, 896, 821, 760 and 686 cm^{-1} in aug-cc-pVDZ basis set.

The aromatic C–H stretching vibrations are observed in the region 3100–300 cm^{-1}, C–H in–plane bending modes (β) are observed in the range 1300–850 cm^{-1} and C–H out–of–plane bending modes (γ) are observed in the range 950–600 cm^{-1}. In 5B1HT, the aromatic C–H stretching vibrations are observed from mode 2 to mode 8. The C–H stretching vibrations are observed at 2863 and 2826 m^{-1} in the experimental FT–Raman spectrum and from mode 2 to mode 6 and the scaled theoretical wavenumbers are observed at 3087, 3077, 3068, 3060 and 3057 cm^{-1} at 6311++G(d,p) basis set. The in–plane bending modes for C–H vibrations are observed at mode numbers 11, 13, 14, 16, 22 and 23. The in–plane bending modes for C–H vibrations are observed at 1539 and 1153 cm^{-1} in the FTIR spectrum and observed at 1434 cm^{-1} in the FT–Raman spectrum. The C–H torsion vibrational modes are observed at mode numbers 31, 34, 36, 38 and 40 and observed at 976, 925 and 759 cm^{-1} in the FTIR spectrum and observed at 893 and 727 cm^{-1} in the FT–Raman spectrum. The observed vibrational modes are matched with the literature [55, 56].

In the FT-IR spectra of benzyl thiocyanide, we were measured at 2145.38 cm^{-1} in the 2500 cm^{-1} region. This peak is part of the -CN group [57,58]. In this work, the C–N stretching vibrations are observed at mode numbers 12, 15, 20, 27 and 32 as given in Table 1 and observed at 963 cm^{-1} in the experimental Raman spectrum. The N–H in–plane bending vibrations are observed at mode numbers 12, 15 and 20. The N–N stretching vibrations are observed at mode numbers 17, 20, 26 and 29 where mode 17 shows 58% of N–N stretching at 1297 cm^{-1} at 6–311++G(d,p) basis set and at 1043 cm^{-1} in the FT–IR spectrum and 994 cm^{-1} in the Raman spectrum. The N–H torsion vibrations are observed at mode 41 at 677 cm^{-1} [59, 60].

Overall, because the band has a variable intensity, the assignment of the band due to the carbon-sulfur (C-S) stretching vibration is difficult to see in FT-IR spectra. These peaks can be found in the 1030.23-200 cm^{-1} range [61]. For title compound, there are four C-S stretches. The standard mode numbers are 42, 44, 46 and 47. The 46 mode shows 46% C-S stretching. For the B3LYP/6-311++G(d,p) level of theory, the 46th mode is predicted at 482 cm^{-1}. Other stretching vibrations are interacting with bending and stretching vibrations. In the DFT (6-311++G(d,p) basis sets) calculation, CS vibrations with mixing other bending and stretching are determined in the 445-465 cm^{-1} region. These peaks were not measured in the FT-IR spectra. Infrared spectra typically show characteristic vibration peaks for free tetrazole groups at 1639.9-1340 and 1200-900 cm^{-1} [62, 63].

The peak of NN stretching vibrations is determined to be 1329.03 cm^{-1}. In the Infrared spectra, the CH_2 scissoring vibrations are measured at 1432 cm^{-1} at mode 14. This peak is associated with the S-CH_2 group's scissoring vibrations [64]. The observed frequencies are in good agreement with previously reported FT-IR spectra. The observed and calculated frequencies are found to be very close. The C–S torsion modes are observed at mode numbers 35, 55, 56 and 57. The out–of–plane N–S bending is observed at mode numbers 41 and 51.

Table 1– Computed and observed vibrational assignments of N26D1P atB3LYP/cc–pVDZ and B3LYP/ 3–21G basis sets [*v*– stretching, *β*–in–plane bending, *γ*– out of plane bending, *τ*–Torsion, vw– very weak, w– weak, m– medium, s– strong, vs– very strong].

Mode No.	Observed Wavenumber (cm^{-1})		B3LYP/6311++G(d,p) Calculated wavenumber		B3LYP/CCPVDZ Calculated wavenumber		Probable Assignments (>10%)
	FTIR	RAMAN	Unscaled	Scaled	Unscaled	Scaled	
1			3649	3529	3642	3533	νN_1-H_6(100)
2			3192	3087	3201	3105	νC_{14}-H_{19}(26)+ νC_{16}-H_{20}(26)+ νC_{18}-H_{21}(40)
3			3182	3077	3191	3095	νC_{14}-H_{19}(41)+ νC_{16}-H_{20}(40)
4			3173	3068	3182	3087	νC_{12}-H_{15}(20)+ νC_{13}-H_{17}(21)+ νC_{18}-H_{21}(46)
5			3164	3060	3173	3078	νC_{12}-H_{15}(39)+ νC_{13}-H_{17}(41)+ νC_{16}-H_{20}(10)
6			3161	3057	3170	3075	νC_{12}-H_{15}(27)+ νC_{13}-H_{17}(24)+ νC_{14}-H_{19}(18)+ νC_{16}-H_{20}(17)+ νC_{18}-H_{21}(14)
7		2863(m)	3148	3044	3161	3066	νC_8-H_9(49)+ νC_8-H_{10}(50)
8		2826(vw)	3091	2989	3096	3003	νC_8-H_9(50)+ νC_8-H_{10}(49)
9	1710(vs)		1644	1590	1647	1598	νC_{12}-C_{14}(30)+ νC_{16}-C_{13}(10)
10	1603(s)	1613(w)	1624	1570	1626	1577	νC_{18}-C_{16}(28)+ νC_{13}-C_{11}(22)+βC_{12}-C_{14}-C_{18}(10)
11	1539(vs)		1526	1476	1515	1470	βH_{15}-C_{12}-C_{14}(15)+ βH_{17}-C_{13}-C_{16}(15)+ βH_{19}-C_{14}-C_{18}(17)+ βH_{20}-C_{16}-C_{18}(17)
12	1515(m)	1498(w)	1502	1452	1503	1458	νN_4-C_5(17)+ νN_1-C_5(12)+ βH_6-N_1-N_2(42)
13		1434(vs)	1484	1435	1472	1428	βH_{19}-C_{14}-C_{18}(11)+βH_{20}-C_{16}-C_{18}(11)+ βH_{21}-C_{18}-C_{16}(26)
14			1481	1432	1456	1412	βH_{10}-C_8-H_9(79)
15	1327(m)		1377	1332	1383	1342	νN_4-C_5(47)+νN_1-C_5(18)+βN_2-N_1-C_5(12)
16			1359	1314	1354	1313	βH_{15}-C_{12}-C_{14}(27)+ βH_{17}-C_{13}-C_{16}(27)+ βH_{19}-C_{14}-C_{18}(10)+ βH_{20}-C_{16}-C_{18}(10)+ βH_{21}-C_{18}-C_{16}(10)
17			1341	1297	1341	1301	νN_3-N_2(58)
18			1339	1295	1340	1300	νC_{12}-C_{14}(17)+ νC_{14}-C_{18}(18)+νC_{16}-C_{13}(17)+νC_{13}-C_{11}(24)

19			1279	1237	1264	1226	νC_{11}-C_8(10)+ βH_{10}-C_8-H_9(16)+τH_9-C_8-S_7-C_5(23)+ τH_{10}-C_8-S_7-C_5(35)
20			1241	1200	1239	1202	νN_3-N_2(20)+ νN_1-C_5(16)+ βH_6-N_1-N_2(33)
21			1225	1185	1220	1183	νC_{11}-C_8(35)
22			1204	1164	1195	1159	βH_{15}-C_{12}-C_{14}(21)+ βH_{17}-C_{13}-C_{16}(21)+ βH_{19}-C_{14}-C_{18}(17)+ βH_{20}-C_{16}-C_{18}(17)
23	1153(m)		1184	1145	1173	1138	βH_{19}-C_{14}-C_{18}(19) +βH_{20}-C_{16}-C_{18}(19) + βH_{21}-C_{18}-C_{16}(39)
24			1152	1114	1138	1104	βH_9-C_8-S_7(46)+ τH_{10}-C_8-S_7-C_5(23)
25			1097	1061	1092	1059	νC_{12}-C_{14}(13)+ νC_{16}-C_{13}(14)+ βH_9-C_8-S_7(17)+ βH_{21}-C_{18}-C_{16}(11)
26	1043(w)		1078	1042	1084	1051	νN_2-N_1(24)+ βN_3-N_2-N_1(60)+ βN_2-N_1-C_5(11)
27			1056	1021	1053	1021	νN_4-C_5(17)+βN_4-C_5-N_1(15)+ βN_2-N_1-C_5(44)
28	1016(w)		1049	1014	1047	1016	νC_{14}-C_{18}(21)+ νC_{18}-C_{16}(20)+βC_{12}-C_{14}-C_{18}(13)+ βH_{19}-C_{14}-C_{18}(11)+βH_{20}-C_{16}-C_{18}(11)
29		994(vw)	1023	989	1033	1002	νN_2-N_1(65)+βH_6-N_1-N_2(11)+βN_3-N_2-N_1(10)
30			1018	984	1010	980	νC_{14}-C_{18}(13)+νC_{18}-C_{16}(11)+βC_{12}-C_{14}-C_{18}(27)+ βC_{14}-C_{18}-C_{16}(20)+ βC_{18}-C_{16}-C_{13}(13)
31	976(w)		1003	970	999	969	τH_{19}-C_{14}-C_{18}-C_{16}(21)+ τH_{20}-C_{16}-C_{18}-C_{14}(20)+ τH_{21}-C_{18}-C_{16}-C_{13}(36)+ τC_{14}-C_{18}-C_{16}-C_{13}(11)
32		963(vw)	990	957	998	968	νN_1-C_5(35)+ βN_4-C_5-N_1(44)
33	951(w)		986	953	980	951	τH_{15}-C_{12}-C_{14}-C_{18}(18)+ τH_{17}-C_{13}-C_{16}-C_{18}(18)+ τH_{19}-C_{14}-C_{18}-C_{16}(27)+ τH_{20}-C_{16}-C_{18}-C_{14}(28)
34	925(m)	893(w)	934	903	924	896	τH_{15}-C_{12}-C_{14}-C_{18}(28)+ τH_{17}-C_{13}-C_{16}-C_{18}(28)+ τH_{21}-C_{18}-C_{16}-C_{13}(29)
35			900	870	893	866	βH_9-C_8-S_7(30)+ τH_9-C_8-S_7-C_5(41)
36			855	827	846	821	τH_{15}-C_{12}-C_{14}-C_{18}(26)+ τH_{17}-C_{13}-C_{16}-C_{18}(26)+ τH_{19}-C_{14}-C_{18}-C_{16}(23)+ τH_{20}-C_{16}-C_{18}-C_{14}(23)

37			826	799	825	800	νC_{11}-C_8(20)+βC_{14}-C_{18}-C_{16}(32)
38	759(m)	727(w)	785	759	784	760	τH_{19}-C_{14}-C_{18}-C_{16}(10)+ τH_{20}-C_{16}-C_{18}-C_{14}(10)+ τH_{21}-C_{18}-C_{16}-C_{13}(10)+ τC_{18}-C_{16}-C_{13}-C_{11}(26)
39		699(m)	721	697	726	704	τN_4-C_5-N_1-N_2(30)+ τN_3-N_2-N_1-C_5(63)
40			709	686	707	686	τH_{15}-C_{12}-C_{14}-C_{18}(13)+ τH_{17}-C_{13}-C_{16}-C_{18}(13)+ τH_{21}-C_{18}-C_{16}-C_{13}(19)+ τC_{12}-C_{14}-C_{18}-C_{16}(15)+ τC_{14}-C_{18}-C_{16}-C_{13}(10)+ τC_{18}-C_{16}-C_{13}-C_{11}(21)
41			700	677	706	685	τH_6-N_1-N_2-N_3(27)+ τN_4-C_5-N_1-N_2(36)+ τN_3-N_2-N_1-C_5(15)+ γS_7-N_1-N_4-C_5(20)
42			683	660	680	660	νS_7-C_8(41)+ τC_{12}-C_{14}-C_{18}-C_{16}(11)+ τC_{18}-C_{16}-C_{13}-C_{11}(17)
43			635	614	630	611	βC_{12}-C_{14}-C_{18}(24)+ βC_{16}-C_{13}-C_{11}(21)+ βC_{18}-C_{16}-C_{13}(35)
44			578	559	576	559	νS_7-C_8(15)+ βC_{14}-C_{18}-C_{16}(14)+ βC_{16}-C_{13}-C_{11}(19)
45		526(w)	520	503	549	533	τH_6-N_1-N_2-N_3(70)+ τN_3-N_2-N_1-C_5(16)
46			498	482	498	483	νS_7-C_5(47)
47			483	467	485	470	νS_7-C_5(17)+τC_{14}-C_{18}-C_{16}-C_{13}(21)
48		413(vw)	414	400	413	401	τH_{15}-C_{12}-C_{14}-C_{18}(12)+ τH_{17}-C_{13}-C_{16}-C_{18}(12)+ τC_{12}-C_{14}-C_{18}-C_{16}(40)+ τC_{14}-C_{18}-C_{16}-C_{13}(24)
49			335	324	340	330	βC_{13}-C_{11}-C_8(71)
50			328	317	324	314	βS_7-C_5-N_4(56)+βC_8-S_7-C_5(15)
51			245	237	250	243	τN_4-C_5-N_1-N_2(25)+ γS_7-N_1-N_4-C_5(63)
52		176(vw)	238	230	237	230	νS_7-C_8(16)+βC_{11}-C_8-S_7(20)+τC_{14}-C_{18}-C_{16}-C_{13}(11)+ τC_{16}-C_{13}-C_{11}-C_8(20)
53			130	126	129	125	βS_7-C_5-N_4(18)+ βC_8-S_7-C_5(39)+ τC_{16}-C_{13}-C_{11}-C_8(23)
54			62	60	61	59	βC_{11}-C_8-S_7(35)+ βC_8-S_7-C_5(24)+ τC_{16}-C_{13}-C_{11}-C_8(32)
55			59	57	57	55	τC_{13}-C_{11}-C_8-S_7(29)+ τC_8-S_7-C_5-N_1(68)
56			33	32	31	30	τC_{13}-C_{11}-C_8-S_7(68)+ τC_8-S_7-C_5-N_1(28)
57			22	21	18	17	τC_{11}-C_8-S_7-C_5(85)

3.3. NMR Study

Table-2 summarises the calculated and observed ^{13}C NMR and ^{1}H NMR chemical shift values. The calculated values of ^{13}C and ^{1}H chemical shifts in DMSO are summarized using the B3LYP/6- 311++G(d, p) level of theory. Figs. 7 and 8 show the measured ^{1}H and ^{13}C NMR spectra respectively. Table-1 summarises the observed ^{13}C NMR and ^{1}H NMR chemical shift values. The lowest NMR signals in the ^{1}H NMR spectra of the title compound belong to the methylene (CH2) group. These signals were displayed in the 2.01-0.99 ppm range. The singlet peaksat 4.47 and 4.49 ppm in the ^{1}H NMR spectra (Fig. 7) belong to protons of the methylene groups between the aromatic benzene ring and the sulphur atom [65]. DFT calculations predict these chemical shifts at 4.16 ppm (H10) and 4.56 ppm (H9).

Multiple peaks for the -CH group protons of the bounded tetrazole ring were observed in the 5.70-3.14 ppm range. DFT calculates this H6 proton signal at 5.71 ppm. The aromatic protons have ^{1}H NMR signals in the range 7.37-7.18 ppm for the phenyl group. 7.25 ppm (H19), 7.28 ppm (H15), 7.36 ppm (H17), 7.38 ppm (H20) and 7.26 ppm (H21) are the locations of these signals [66]. We calculated 7.83 ppm (H19), 7.50 ppm (H15), 7.63 ppm (H17), 7.78 ppm (H20) and 8.20 ppm (H21) using the theoretical method. Furthermore, we detected a weak and broad 11 N-H signal from the tetrazole ring at 12.40 ppm in 5-(benzylthio)-1*H*-tetrazole [67]. Tetrazole formation is also supported by the data.

Previous research [68] indicates that the range of ^{13}C NMR chemical shifts for a typical organic molecule is typically greater than 100 ppm, ensuring a reliable interpretation of spectroscopic parameters [69]. The ^{13}C NMR chemical shifts of the tetrazole group for the title compound are greater than 100 ppm in Fig. 8 of the current paper except that for C8. The signal for C8 has been observed at 38.86 ppm in experimental spectra and at 42.62 in theoretical calculation. The experimental spectra show these signals in the 128.17-154.26 ppm range. Using theoretical calculations, the chemical shifts are observed at 132.5 (C12), 132.7 (C13), 133.2 (C14), 133.7 (C16), 134.8 (C18) and 148.9 (C11). The observed and calculated ^{13}C NMR signals are found to be in good agreement, as shown in Table-1. The tetrazole group has a 154.26 ppm signal and a higher signal in the ^{13}C NMR spectra [70]. The chemical shifts obtained for the 1H atoms are lower than those obtained from the ^{13}C NMR signal of the tetrazole group [71, 72]. All of the signals are less than 100 ppm. Other signals are calculated in the 36.55-40.62 ppm range and measured between 25.72 and 38.76 ppm [73]. Weak signals of 16.54 and 2.44 ppm are also detected [74,75]. The observed signals are found to be in good agreement with the NMR spectra.

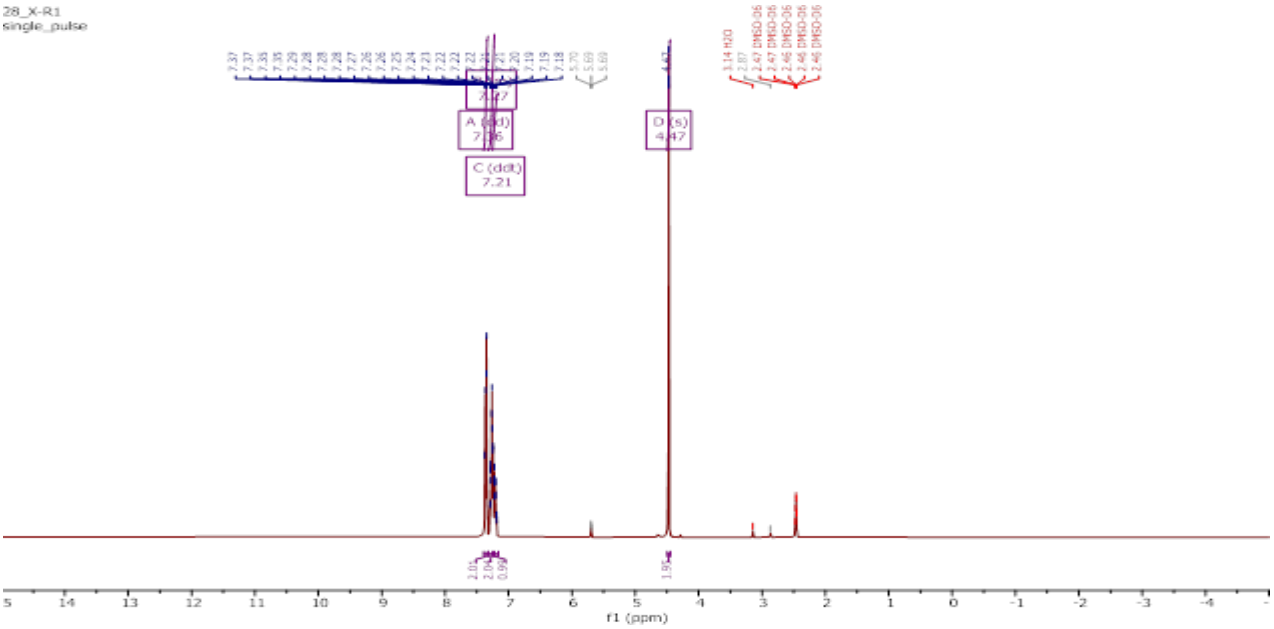

Fig. 7. ^{1}H NMR spectra of 5BIHT

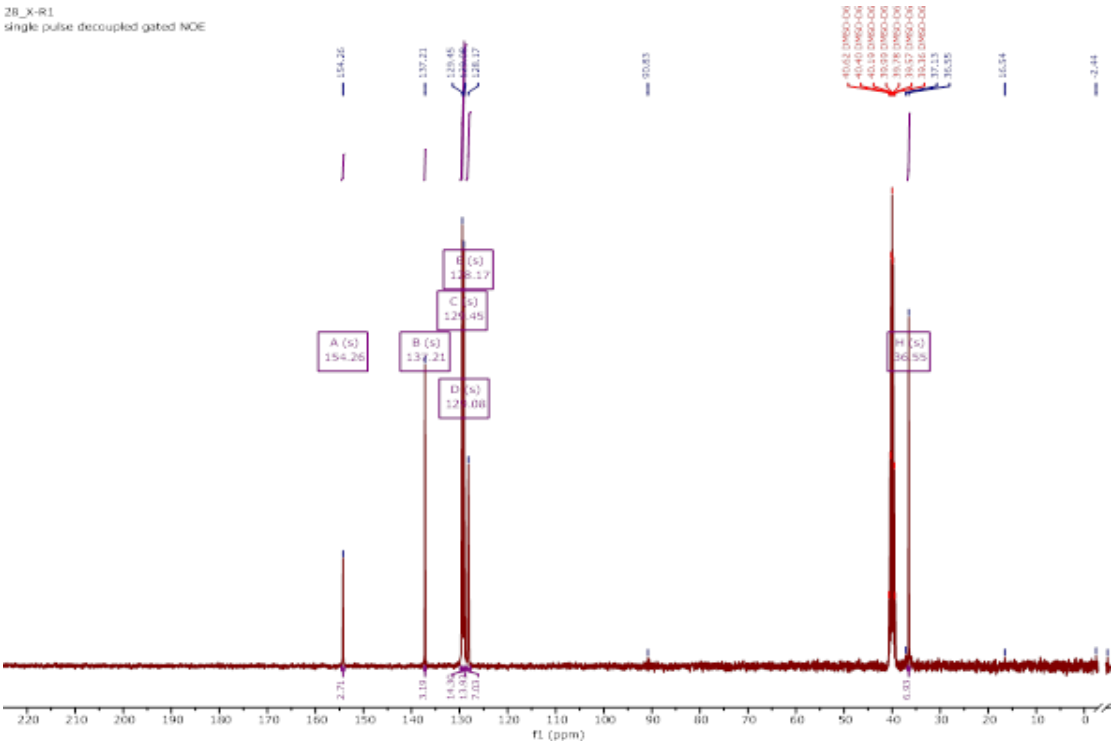

Fig. 8. ^{13}C NMR spectra of 5B1HT

Table-2 The observed and predicted 1H and ^{13}C NMR isotropic chemical shifts (with respect to TMS, all valuesin ppm) f

Atom numbering	Theoretical	Experimental
C_8	42.62	38.86
C_{12}	132.5	126.05
C_{13}	132.7	126.05
C_{14}	133.2	128.08
C_{16}	133.7	128.08
C_{18}	134.8	129.01
C_{11}	148.9	137.81
C_5	128.5	126.4
H_9	4.56	4.49
H_{10}	4.16	4.47
H_6	5.71	5.70
H_{19}	7.83	7.25
H_{15}	7.50	7.28
H_{17}	7.63	7.36
H_{20}	7.78	7.38
H_{21}	8.20	7.26

4. Conclusion

First, we synthesized 5-(benzylthio)1*H*-tetrazole (5B1HT). Data from powder XRD, FT-IR, FT-Raman, SEM, UV-Vis and NMR spectroscopy were collected and analyzed. The 5B1HT molecule was subjected to nuclear, conformational, structural and theoretical analysis using Gaussian 09 and Spartan 10 software. Theoretical and experimental NMR and FT-IR spectral results were compared. The experimental NMR chemical shifts and FT-IR spectra peaks matched the theoretical values very well. In medicinal chemistry, the tetrazole heterocycle is an important moiety. It can mimic enzymatic targets due to its similarities to the cis-amide and carboxylic acid functionalities and it has a wide range of biological activities such as antiviral, antifungal, antibacterial and antihypertensive activities. Several other synthetic routes have also been demonstrated to be efficient and cost-effective; however, these pathways must still be optimized in order to produce a more diverse set of final products.

Conflict of Interest

No conflict of interest among the authors.

References:

1. Zou, Y., Liu, L., Liu, J., & Liu, G.. Bioisosteres in drug discovery: Focus on tetrazole. Future Medicinal Chemistry,2020; 12 (2): 91–93. https://doi.org/10.4155/fmc-2019-0288
2. Leyva-Ramos, S., & Cardoso-Ortiz, J. Recent developments in the synthesis of tetrazoles and their pharmacological relevance. Current Organic Chemistry,2021; 25(3):388–403. https://doi.org/10.2174/1385272824999201210193344.
3. Swami, S., Sahu, S. N., & Shrivastava, R. Nanomaterial catalyzed green synthesis of tetrazoles and its derivatives: A review on recent advancements. RSC Advances,2021; 11(62): 39058–39086. https://doi.org/10.1039/D1RA05955F
4. Safapoor, S., & Mohammad, G. (2022). Dekamin, ArezooAkbari and M. Reza Naimi-Jamal, Synthesis of (E)-2-(1H- tetrazole- 5-yl)-3- phenylacrylenenitrile derivatives catalyzed by new ZnO nanoparticles embedded in a thermally stable magnetic periodic mesoporous organosilica under green conditions. http://doi.org/10.1038/s41598-022-13011-9, 12(10723).
5. M. Nasrollahzadeh Sajjadi, M., Tahsili, M. R., Shokouhimehr, Mohammadreza, & Varma, R. S., Synthesis of 1substituted.1H-1,2,3,4-Tetrazoles Using Biosynthesized Ag/Sodium Borosilicate Nanocomposite. ACS Omega, 2019, 4 (5): 8985–9000. https://doi.org/10.1021/acsomega.9b00800.
6. Keglevich, G. (2021) Current Organic Chemistry, 25(1), 1–16. DOI: 10.2174/1385272825012101011616l5.
7. Aouine, Y., Jmiai, A., Alami, A., El Asri, A., El Issami, S., & Bakas, I. (2021). Experimental and computational studies on N -alkylation reaction of N-benzoyl 5-(aminomethyl)tetrazole. Chemistry, 2021; 3(3), 704–713. https://doi.org/10.3390/chemistry3030049.
8. Myznikov, L. V., Vorona, S. V., & Zevatskii, Y. E. Biologically active compounds and drugs in the tetrazole series. Chemistry of Heterocyclic Compounds, 2021;57(3), 224–233. https://doi.org/10.1007/s10593-021-02897-4.
9. Bayannavar, P. K., Kamble, R. R., Joshi, S. D., Nesaragi, A. R., Shaikh, S. K. J., Sudha, B. S., Dodamani, S. S., & Hoolageri, S. R. Design and synthesis of angiotensin converting enzyme (ACE) inhibitors: Analysis of the role of tetrazole ring appended to biphenyl moiety. Chemistry Select,2022; 7(2), e202103336. https://doi.org/10.1002/slct.202103336
10. Ballatore, C., Huryn, D. M., & Smith, A. B., III. (2013). Carboxylic acid (bio)isosteres in drug design. ChemMedChem,2013; 8(3), 385–395. https://doi.org/10.1002/cmdc.201200585.
11. Mittal, R., & Awasthi, S. K. Recent advances in the synthesis of 5-substituted 1H-Tetrazoles: A complete survey (2013–2018). Synthesis,2019; 51(20), 3765–3783. https://doi.org/10.1055/s-0037-1611863
12. Khamooshi, F., Anti-HIV drugs study: Study of NNRTIs function and overview synthesis of specific and rare aryloxy tetrazoles derivatives as NNRTIs and anti-HIV drug. Medicon Pharmaceutical Sciences, 2022; 2(3), 04–10.
13. Sonkar, C., Malviya, N., Sinha, N., Mukherjee, A., Pakhira, S., & Mukhopadhyay, S. Selective anticancer activities of ruthenium(II)-tetrazole complexes and their mechanistic insights. Biometals,2021; 34(4), 795–812. https://doi.org/10.1007/s10534-021-00308-x
14. Popova, E. A., Trifonov, R. E., & Ostrovskii, V. A. Tetrazoles for biomedicineElena. Russian Chemical Reviews,2019; 88(6), 644–676. https://doi.org/10.1070/RCR4864
15. Duddigan, S., Alexander, P. D., Shaw, L. J., & Collins, C. D. Effects of repeated application of organic soil amendments on horticultural soil physicochemical properties, nitrogen budget and yield. Horticulturae,2021; 7(10), 371. https://doi.org/10.3390/horticulturae7100371
16. Li, Y. T., Yao, W. Q., Zhou, S., Xu, J. X., Lu, H., Lin, J., Hu, X. Y., & Zhang, S. K. Synthesis, fungicidal activity and 3D -QSAR of tetrazole derivatives containing phenyloxadiazole moieties. Bioorganic and Medicinal Chemistry Letters,2021; 34, 127762. https://doi.org/10.1016/j.bmcl.2020.127762. Epub December 24 2020. PubMed: 33359605
17. Arlt, A. schwarz-georg cancho grande, yolanda füßlein, martin jeschke, peter ebbinghaus kintscher, ulrich linka, marc, lösel, peter damijonaitis, arunas jonas, turberg andreas heisler, iring, mandzhulo, Oleksandr, Novel Heteroaryl-Triazole Compounds As Pesticides. accessed on 28.01.2021, WO/2021/013720, https://patents.google.com/patent/WO2021013720A1/en.
18. Kyarikwal, R., Malviya, N., Chakraborty, A., & Mukhopadhyay, S. Preparation of Tris-tetrazole-based Metallogels and stabilization of silver nanoparticles: Studies on reduction catalysis and self-healing property. ACS Applied Materials and Interfaces,2021; 13(49), 59567–59579. https://doi.org/10.1021/acsami.1c19217
19. Abdessalam, M., Sidhoum, M. A., Zradni, F.-Z., & Ilikti, H. Synthesis of 1,5-disubstituted tetrazoles in aqueous micelles at room temperature. Molbank, 2021(1). https://doi.org/10.3390/M1194
20. Pirota, V., Benassi, A., & Doria, F. Lights on 2,5-diaryl tetrazoles: Applications and limits of a versatile photoclick reaction. Photochemical and Photobiological Sciences,2022; 21(5), 879–898. https://doi.org/10.1007/s43630-022-00173-8
21. Rama, V., Kanagaraj, K., & Pitchumani, K.Syntheses of 5-substituted 1H-Tetrazoles catalyzed by reusable CoY zeolite. Journal of Organic Chemistry, 2011;76(21), 9090–9095. https://doi.org/10.1021/jo201261w
22. Sandmann, G., Schneider, C., & Böger, P. A new non-radioactive assay of phytoene desaturase to evaluate bleaching herbicides. Zeitschrift Fur Naturforschung. C, Journal of Biosciences, 1996; 51(7–8), 534–538. https://doi.org/10.1515/znc-1996-7-812.
23. Koldobskii, G.I., Myznikov, Y.E. & Zhivich, A.B. Phase-transfer catalysis in the chemistry of tetrazoles. Chemistry Heterocyclic Compound,1992; 28, 626–631. https://doi.org/10.1007/BF00529333.
24. Muhammed, A., Sreelakshmi, P., Praseed, P. N., Jishnu & Shan S. A review on gas-generants for application in exploding fire extinguisher balls. IOP Conference Series: Materials Science and Engineering, IOP Conference Series: Materials Science and Engineering, 2021; 1114, DOI:10.1088/1757-899X/1114/1/012079/meta.
25. Sandmann, G., Schneider, C., & Böger, P. A new non-radioactive assay of phytoene desaturase to evaluate bleaching herbicides. Zeitschrift Fur Naturforschung. C, Journal of Biosciences, 1996; 51(7–8), 534–538. https://doi.org/10.1515/znc-1996-7-812, PubMed: 8810094
26. Zubarev, V.Y., Ostrovskii, V.A.,Methods for the synthesis of mono- and polynuclear NH-tetrazoles. Chemistry of Heterocyclic Compound,2000; 36, 759–774 https://doi.org/10.1007/BF02256907.
27. Chen, Z., & Xiao, H., Impact sensitivity and activation energy of pyrolysis for tetrazole compounds. International Journal of Quantum Chemistry,2000; 79(6), 350–357. https://doi.org/10.1002/1097-461X(2000)79:6.

28. A. Go´mez-Zavaglia,,I. D. Reva, L. Frija,, M. L. Cristiano, R. Fausto,Molecular Structure, Vibrational Spectra and Photochemistry of2-Methyl-2H-Tetrazol-5-Amine in Solid Argon, Journal of Physical Chemistry. 2005;109,7967-7976. Doi: 10.1021/jp0517706.
29. Balabina R.M., Tautomeric equilibrium and hydrogen shifts in tetrazole and triazoles: Focal-point analysis and ab initio limit, Journal of Chemical Physics,2009; 131, 154307.https://doi.org/10.1063/1.3249968.
30. Goddard, R., Heinemann, O., & Kru, C. Ager. Acta Crystallographica, Section C, 1997;53, 590–592.
31. Butler, R. N., Garvin, V. C., Lumbroso, H., & Lie'geois, C. Journal of the Chemical Society. Perkin Transactions Rans, 1984;2, 721.
32. Zhaoxu, C., & Heming, X. Journal of Molecular Structure (T heochem.),1998; 453(1–3), 65–70. https://doi.org/10.1016/S0166-1280(98)00177-8
33. 34, Mazurek, A. P., Sadlej-Sosnowska, N., & Chem. (2000). Phys. L Ett, 212, 330.
34. Saglam, S., Disli, A., Erdogdu, Y., Marchewka, M. K., Kanagathara, N., Bay, B., & Güllüoğlu, M. T.,Synthesis, characterization and theoretical studies of 5-(benzylthio)-1-cylopentyl-1*H*-tetrazole. Spectrochimica Acta. Part A: Molecular and Biomolecular Spectroscopy.2014; https://doi.org/10.1016/j.saa. 2014.07.071.
35. Hohenberg, P., & Kohn, W.,Inhomogeneous electron gas. Physical Review, 1964; 136(3B), B864–B871.https://doi.org/10.1103/PhysRev.136.B864
36. Kohn, W., & Sham, L. J.,Self-consistent equations including exchange and correlation effects. Physical Review,1965; 140(4A), A1133–A1138 [DOI: 10.1103/PhysRev.140.A1133, https://doi.org/10.1103/PhysRev.140.A1133
37. Spartan., 2010, 10 p. 92612. Wavefunction, Inc.
38. Rauhut, G., & Pulay, P.,Transferable scaling factors for density functional derived vibrational force fields. Journal of Physical Chemistry,1995; 99(10), 3093–3100 [DOI: 10.1021/j100010a019, https://doi.org/10.1021/j100010a019
39. Güllüoğlu, M. T., Erdogdu, Y., Karpagam, J., Sundaraganesan, N., & Yurdakul, Ş., DFT, FT-Raman, FT-IR and FT NMR studies of 4-phenylimidazole. Journal of Molecular Structure, 2011; 990(1–3), 14–20 [DOI: 10.1016/j.molstruc.2011.01.001, https://doi.org/10.1016/j.molstruc.2011.01.001
40. Erdogdu, Y., Güllüoğlu, M. T., Yurdakul, S., & Dereli, Ö.,DFT simulations, FT-IR, FT-Raman and FT NMR spectra of 4-(4-chlorophenyl)-1*H*-imidazole molecules. Optics and Spectroscopy,2012; 113(1), 23–32 [DOI: 10.1134/S0030400X12070089, https://doi.org/10.1134/S0030400X12070089
41. Recent Advances in the Synthesis of 5-Substituted 1H-Tetrazoles:A Complete Survey (2013–2018); R. Mittal, S. K. Awasthi—Synthesis, 2019, 51, 3765–3783, DOI: 10.1055/s-0037-1611863
42. Erdogdu, Y., Manimaran, D., Güllüoğlu, M. T., Amalanathan, M., Joe, I. H., & Yurdakul, Ş.. Optics and Spectroscopy,2013; 114, 46–57.
43. Sajedeh Safapoor, MohammadG. Dekamin*, ArezooAkbari & M. Reza Naimi- Jamal, Synthesis of (E) 2 (1H tetrazole 5 yl) 3 phenylacrylenenitrile derivatives catalyzed by new ZnO nanoparticles embedded in a thermally stable magnetic periodic mesoporous organosilica under green conditions, Scientifc Reports, 2022; 12:10723, https://doi.org/10.1038/s41598-022-13011-9.
44. Erdogdu, Y. Spectrochimica Acta, Part A, 2013;106, 25–33.
45. Ozısık, H., Saglam, S., & Bayarı, S. H.,Molecular structure and vibrational spectra of 4-, 5-, 6-chloroindole. Structural Chemistry,2008; 19(1), 41–50. https://doi.org/10.1007/s11224-007-9247-x
46. Yazdani, A., Höhne, G. W. H., Misture, S. T., & Graeve, O. A.,A method to quantify crystallinity in amorphous metal alloys: A differential scanning calorimetry study. PLOS ONE. PubMed,2020; 15(6), e0234774. https://doi.org/10.1371/journal.pone.0234774
47. Sokolova, M. M., MelĬnikov, V. V., Ostrovskii, V. A., Koldobskii, G. I., MelĬnikov, A. A., & Gidaspov, B. V. Zhurnal Organicheskoi Khimii, 1975;11, 1744.
48. Baglin, F. G. External optic phonons in tetrazole. Journal of Chemical Physics,1972; 56(1), 358–361. DOI: 10.1063/1.1676873.
49. Bugalho, S. C. S., Maçôas, E. M. S., Lurdes S. Cristiano, M., & Fausto, R. Low temperature matrix-isolation and solid state vibrational spectra of tetrazole. Physical Chemistry Chemical Physics,2001; 3(17), 3541–3547 [DOI: 10.1039/b103344c, https://doi.org/10.1039/b103344c
50. Kipkemboi, P., Kiprono, P. C., & Sanga, J. J. Vibrational spectra of t-butyl alcohol, t-butylamine and t-butyl alcohol + t-butylamine binary liquid mixtures,Bulletin of the Chemical Society of Ethiopia,2003; 17(2) [DOI: 10.4314/bcse.v17i2.61689.
51. F Billes, H Endrédi, G Keresztury, Vibrational spectroscopy of triazoles and tetrazole, Journal of Molecular Structure: THEOCHEM,2000; 530, Pg 183-200.
52. Mechanochromic luminogens with hypsochromically shifted emission switching property: recent advances and perspectives, Faizal Khan, Anupama Ekbote, Garima Singh and Rajneesh Misra, J. Mater. Chem. C, 2022; 10, 5024-5064. DOI: 10.1039/D1TC06140B.
53. Rosado, M. T. S., Duarte, M. L. T. S., & Fausto, R. Journal of Molecular Structure, 1997;410–411, 343.
54. Světlík, J., Martvoň, A., & Leško, J. Preparation and spectral properties of tetrazoles. Chem. Zvesti, 1979;33, 521–527.
55. Ghatak, A., & Das, M.,The recent progress on supported and recyclable nickel catalysts towards organic transformations: A review. ChemistrySelect. Select Press, 2021;6(15), 3656–3682. DOI: 10.1002/slct.202100727.
56. Rosado, M. T. S., Duarte, M. L. T. S., & Fausto, R, Journal of Molecular Structure, 1997; 410–411, 343.
57. Spectroscopy table. https://www.cpp.edu/~psbeauchamp/pdf/spec_ir_nmr_spectra_tables.pdf. Beauchamp, France p. 1.
58. Ben Smail, R., Chebbi, H., Srinivasan, B. R., & Zid, M. F., Spectroscopic characterization and room-temperature structure of bis(4-aminopyridinium) dichromate. Journal of Structural Chemistry, 2017; 58(4), 724–733.DOI: 10.1134/S0022476617040126.
59. Karthik, G., Premkumar, K., & Senthil Murugan, V.,FT-IR Raman structure, vibrational frequency analysis of fluorobenzyl chloride based of DFT methodcalculation. Journal of Emerging Technologies and Innovative Research JETIR,2018; 5, 338–341.
60. Venkatram Reddy, B., & Gandham, R. R., Vibrational spectra and modified valence force field for N,N′-methylenebisacrylamide. Indian Journal of Pure and Applied Physics, 2008;46:611-616.
61. Rao, C. N. R., Venkataraghavan, R., & Can.,Journal of Chemistry,1964; 42, 43–49.
62. Svetlik, J., Martvon, A., Lesko, J., & Chem., Zvesti,1979; 33, 521–527.
63. Billes, F., Endrédi, H., & Keresztury, G. Vibrational spectroscopy of triazoles and tetrazole. Journal of Molecular Structure: THEOCHEM,2000; 530(1–2), 183–200. https://doi.org/10.1016/S0166-1280(00)00340-7
64. Khan, S. A., Khan, S. B., Khan, L. U., Farooq, A., Akhtar, K., & Asiri, A. M. Fourier transform infrared spectroscopy: Fundamentals and application in functional groups and nanomaterials characterization. In S. Sharma (Ed.), Handbook of materials characterization. 2018;

https://doi.org/10.1007/978-3-319-92955-2. Springer.
65. Xin Liu, Chapter 6: Structural Identification of Organic Compounds- IR and NMR Spectroscopy, (accessed on 6Dec) 2021; https://chem.libretexts.org
66. Subashchandrabose, S., Akhil, R., Krishnan, H., Saleem, V., Thanikachalam, V., Manikandan, G., & Erdogdu, Y., J. Mol. Struc.2010; 59-70.
67. Y. Erdogdu, M.T.Güllüoğlu, M. Kurt. Journal of Raman Spectroscopy, 2010; 40 (2009), 981, 1615–1623.
68. Onchoke KK. Data on GC/MS elution profile, 1H and ^{13}C NMR spectra of 1-, 3- and 6-Nitrobenzo[a]pyrenes. Data Brief. 2019;12;28:104995. doi: 10.1016/j.dib.2019.104995.
69. P. N. Gaponik,O. A. Ivashkevich, Tetrazoles: Synthesis, Structures, Physico-Chemical Properties And Application, Chemical Problems of the development of new materials and Technologies, Minsk, 2003, 193-233.
70. Dayrit, F. M., & de Dios, A. C.,1H and 13C NMR for the Profiling of Natural Product Extracts: Theory and Applications. In E. Sharmin, & F. Zafar (Eds.), Spectroscopic Analyses - Developments and Applications. IntechOpen. 2017;https://doi.org/10.5772/intechopen.71040.
71. Synthesis and Characterization of 5-Substituted 1H-tetrazoles in the Presence of Nano-TiCl4.SiO2, L. Zamania, B. F. Mirjalilia, K. Zomorodianb,S. Zomorodian, S. Afr. J. Chem. 68: 133–137.
72. Sinirlioglu, D., Muftuoglu, A.E. & Bozkurt, A. 5-(methacrylamido)tetrazole and vinyl triazole based copolymers as novel anhydrous proton conducting membranes. J Polym Res, 2013;20, 242. https://doi.org/10.1007/s1.0965-013-0242-1.
73. In silico identification of novel chemical compounds with anti-TB potential for the inhibition of InhA and EthR from Mycobacterium tuberculosis Sajal Kumar Halder, Fatiha Elma, bioRxiv preprint, doi: https://doi.org/10.1101/2020.12.04.411967;
74. Experimental and Computational Studies on N-alkylation Reaction of N-Benzoyl 5-(Aminomethyl)Tetrazole, Younas Aouine, Aaziz Jmiai,Anouar Alami, Abdallah El Asri,Souad El Issami, Idriss Bakas, Chemistry, 2021; 3(3), 704 -713; https://doi.org/10.3390/chemistry3030049.
75. Quareshy M, Prusinska J, Kieffer M, Fukui K, Pardal AJ, Lehmann S, Schafer P, Del Genio CI, Kepinski S, Hayashi K, Marsh A, Napier RM. The Tetrazole Analogue of the Auxin Indole-3-acetic Acid Binds Preferentially to TIR1 and Not AFB5. ACS Chem Biol. 2018; 13(9):2585-2594. doi: 10.1021/acschembio.8b00527.